Spring-Dashpot Vibrational Model for the Investigation of Viscoelasticity in Gelatinous Abrasive Media and Subsequent Control of Parameters for the Blast Polishing of Ti-6Al-4V Alloy

Quintin Oliver de Jongh (quintindejongh@gmail.com)
University of Cape Town https://orcid.org/0000-0001-9354-7803
Ramesh Kuppuswamy
University of Cape Town
Matthew Titus
University of Cape Town

Research Article

Keywords: Blast Polishing, Vibrational Modelling, Viscoelastic, Spring-Damper, Contact Mechanics

Posted Date: March 23rd, 2022

DOI: https://doi.org/10.21203/rs.3.rs-1464965/v1

Spring-Dashpot Vibrational Model for the Investigation of Viscoelasticity in Gelatinous Abrasive Media and Subsequent Control of Parameters for the Blast Polishing of Ti-6Al-4VAlloy

*Quintin de Jongh[1], Ramesh Kuppuswamy[1], Matthew Titus[1]
[1]Advanced Manufacturing Lab, University of Cape Town, Cape Town, South Africa
[1*]djnqui001@myuct.ac.za

* Corresponding Author
ORCID ID: 0000-0001-9354-7803

Abstract. Blast polishing offers an operator-friendly solution to many of the previously encountered polishing difficulties. However, the process lacks studies into the control of key parameters, one of which is viscoelasticity (particularly present in biological based abrasive medias). Together with analytical-empirical models, a vibrational spring-dashpot model is presented, which attempts to characterize the impact force, contact time and damping ratio/coefficient of polishing media upon impact; as well as the effects of damping on contact parameters (stress, deformation, and area of contact). Impact force is shown to decrease dramatically with increasing hydration but increases linearly with an increase in kinetic energy. Contact time results show an exponential increase as hydration is increased and show a logarithmic decrease (to a limit) as kinetic energy is increased. Findings show that higher hydration levels result in lower damping ratios (with all results showing that underdamping is present). Higher kinetic energies show a decrease in damping ratio. Similarly, media damping coefficients decrease with both hydration increases and kinetic energy increases. Results show that contact stress is reduced at higher hydration levels (due to higher contact areas and lower forces) and that hydration acts to prevent brittle failure from occurring on the workpiece surface. The findings stipulated provide a base on which to further characterize the process and will help in development and further optimization of the blast polishing process.

Keywords: Blast Polishing, Vibrational Modelling, Viscoelastic, Spring-Damper, Contact Mechanics

MAP: Magnetic Abrasive Polishing
SLS: Standard Linear Solid
AFM: Atomic Force Microscopy
SLM: Selective Laser Melted
TMD: Tuned Mass Damper

1 Introduction

Advanced manufacturing is highly applicable in industry where tolerances are becoming smaller and materials harder to manipulate. Finishing processes, such as polishing, are critical to providing desired material properties, finishes, lessening corrosion and to extending service life. This is applicable to many modern industries (aero-space, biomedical and advanced automotive). Creating a controllable process is censorious to efficiency and optimization in industry, allowing for the inherent saving of resources and time. A controllable process (where outputs can be controlled via process inputs/parameters) is much more attractive to businesses and often means an easier to use machine can be developed.

Blast polishing (also known as Aerolap polishing [1]) is a mechanical finishing manufacturing process that allows for the achievement of a fine surface roughness (of less than 0.1 μm [2]). Other polishing techniques (including MAP, laser polishing and electropolishing) involve either a large amount of operator experience, high process cost, high abrasive media costs, are limited in shape/material compatibility, or the process parameters are difficult to control [1] [3] [4]. The blast polishing process offers a solution to these encountered problems by reducing the required operator experience and background knowledge to a minimum, as well as by reducing process costs and increasing material/shape compatibility. The blast polishing action occurs by means of ductile failure, where asperity peaks fold into the valleys, causing flattening and subsequent smoothening [5].

The polishing process has had many attempts at characterization but has often relied on critical assumptions and simplifications due to the lack of practical experience and experimental results. Analytical models based on the notion of momentum require that the time of contact be broadly estimated, while empirical models require a large number of experimental results and can ignore some scientific rules. Both types of modelling (which are often the inputs of most simulation models) often ignore the important factor of abrasive viscoelasticity upon impact (particularly for bio-media cores such as agar and gelatin).

A vibrational model, using a spring-dashpot system (Kelvin-Voigt type model) is developed, and presented, to aid in the understanding of abrasive media viscoelasticity, which varies as a function of the water content of the media. A previously developed force model (by the authors of this paper) [6] has been modified and extended to allow for the estimation of forces at varying hydration levels and elastic moduli.

The outputs of the model presented in this paper are expected to support the further development of the blast polishing process by allowing for optimization and by providing more defined and controllable process parameters. This will have direct implications and benefits for the manufacturing and advanced manufacturing industries, as the process will become more viable to industry and easier to implement. Experiments regarding forces in blast polishing are lacking and models of viscoelasticity for the blast polishing process have not been presented before, thus the results presented here are of importance to the study of both the polishing process and as well as the Ti-6Al-4V material.

Damper models are present throughout modern research as a means of improving manufacturing process design. Wang et al. [7] optimized the chatter control of a cutting tool by using a mass damper model (using a Euler-Bernoulli beam), finding the optimal required position for a TMD on the tool. Naghieh et al. [8] developed a viscoelastic contact model for layered contact using an SLS model, deriving equations for non-dimensional contact radius and contact pressure (for both a layered and incompressible model).

Finite element models have been used extensively to model viscoelastic impact problems. A notable solution is of that provided by Assie et al. [9], who provide a low-velocity (<30m/s) model for the analysis of a viscoelastic structure contact. The authors used a Wiechart (SLS) model to simulate the internal damping occurring within the structure [9]. This is because the Wiechart model describes both creep and relaxation adequately. The problem is converted into a static problem by use of the Newmark Method and the Lagrange multiplier technique is used to incorporate the contact condition [9].

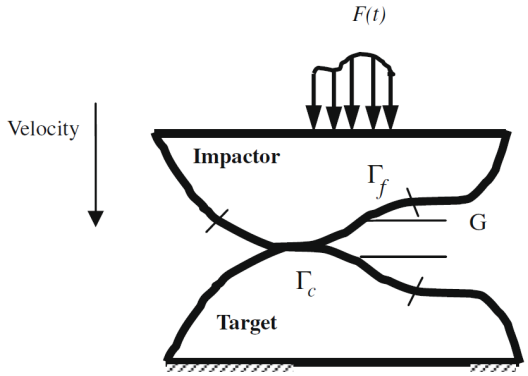

Fig 1. *Viscoelastic Contact Model Source: Assie et. Al [9]*

Their solution involved three phases with multiple steps each. The preprocessor phase involves the input of data: material data, time increment and steps, suitable element, mesh generation, initial conditions, boundary conditions, total contact nodes, contact constraints and input history [9]. The processor phase is more complex and involves generating matrices for stiffness, mass, damping and load vector, before applying constraints and solving for the required output [9]. The postprocessor phase involves repetition and storing material history [9]. Solutions were acquired for one-, two- and three-dimensional problems (for force and displacement) and these lined up well with classical viscoelastic models used by other researchers [10] [11].

FEM, however, is not the only technique used to model viscoelastic contacts and other techniques (including empirical analysis and simulation) have also been

implemented by researchers in the field. Lopez-Guerra and Solares [12] executed multiple approaches to AFM simulation (varying from a simple linear spring dash-pot system to a nonlinear system capable of accurately reproducing viscoelastic surface properties). The response was once again analyzed in terms of force-displacement curves as well as dissipated energy. By analyzing the various spring-dashpot models, the authors were able to highlight strengths and deficiencies that occurred while in contact with the AFM tip.

Fukumoto et al. [13] presented extensive research (mostly experimental) on the blast polishing process. In their third report, they displayed a large set of results regarding the influence of water content in polishing media and how it affects the process. The authors were polishing tungsten carbide surfaces and used polishing hydration levels of 10%, 30% and 50%, impacting at velocities of 55.8 m/s, 48.7 m/s and 41m/s, respectively. They used a high-speed camera (250000 frames/second) to measure the impact time of various hydrated media and found that contact time increased significantly from a wetness of 10% (approximately 10μs) to a wetness of 50% (approximately 70μs) [13]. They thus found that measured impact force decreased significantly (from 2N to 0.5N for 10% hydration and 30% hydration respectively).

Another method of spring-damper modelling is that of the ever-present viscoelastic models. Many are available but the most fitting model applicable to this scenario is that of Kelvin-Voigt's (see **Fig 2** below), as the instantaneous contact only exhibits creep and not stress relaxation.

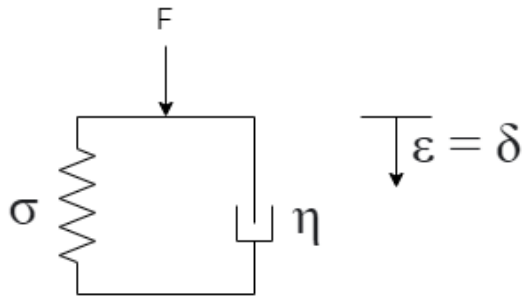

***Fig 2** - Kelvin-Voigt Viscoelasticity Model*

The Kelvin-Voigt model is characterised by the equation below, where strain is equivalent in the damper and the spring, but the total stress is the sum of the stress experienced in the spring and the stress experienced in the damper) [14].

$$\sigma(t) = E\varepsilon(t) + \eta\frac{d\varepsilon(t)}{dt} \tag{1}$$

This is then solved to:

$$\varepsilon(t) = \frac{\sigma_0}{E}\left(1 - e^{-t/\tau_R}\right) \tag{2}$$

Where:

$$\tau_R = \frac{\eta}{E} \tag{3}$$

σ is the stress experienced, t is time, ε is strain experienced, σ_0 is initial stress, η is viscosity of the damper, τ_R is retardation time [14].

Proper calculation of contact time is of utmost importance when developing a force control model or attempting to describe process parameters such as contact stress and deformation. Using the principle of momentum conservation is a popular method to calculate contact time [1], and results line up well with experimentally observed contact times.

An interesting paper by Roberts et al. [15] shows the measurement of contact time in short duration sports ball impacts (which is very similar in nature to the impact of an assumed spherical abrasive with a harder workpiece). A golf ball is assumed hit by a Titanium golf head and this makes the study even more relevant to this proposed model. Hocknell [16] showed that a reasonable estimated of impact duration (contact time) could be made using the following formula derived from Hertz Law (adapted by Goldsmith [17]):

$$\tau = 4.53\left[\frac{m_B(\delta_A+\delta_B)}{\sqrt{R_B v_{imp}}}\right]^{\frac{2}{5}} \tag{4}$$

Where:

$$\delta_A = \frac{1-\nu_A^2}{\pi E_A} \quad (5)$$

And

$$\delta_B = \frac{1-\nu_B^2}{\pi E_B} \quad (6)$$

Where the subscript B denotes the abrasive and A denotes the workpiece.

m is the abrasive mass, R is the radius of abrasive, v_{imp} is impinging velocity, ν is the Poisson ratio of each respective material and E is the elastic modulus of each respective material.

Section 2.1 describes the experimental set-up of the polishing system to gather impact force data (as well as a description of the created polishing machine). This leads to Section 2.2, which describes the empirically measured data and its corresponding regression formula. Section 3 describes the previously developed force model (adapted for hydration), which provides preliminary results for comparison, but mainly provides inputs for Section 4. In Section 4, the results of the vibrational model are presented and discussed in relation to previously developed models and understandings of the process. Finally, conclusions are presented in Section 5.
To note: besides for the data acquisition (done in DeweSoft X3); all modelling, graphing and analysis, was completed in MATLAB R2021a.

2 Experimental Procedure

2.1 Experimental Procedure

A machine was developed to impart ductile regime polishing conditions to a work-piece. Process modelling to predict forces and to aid in design of the machine were completed [6] using analytical, semi-analytical-empirical and simulation methods. Process testing was completed, and results were positive, with surface roughness decreasing exponentially over time (as expected).

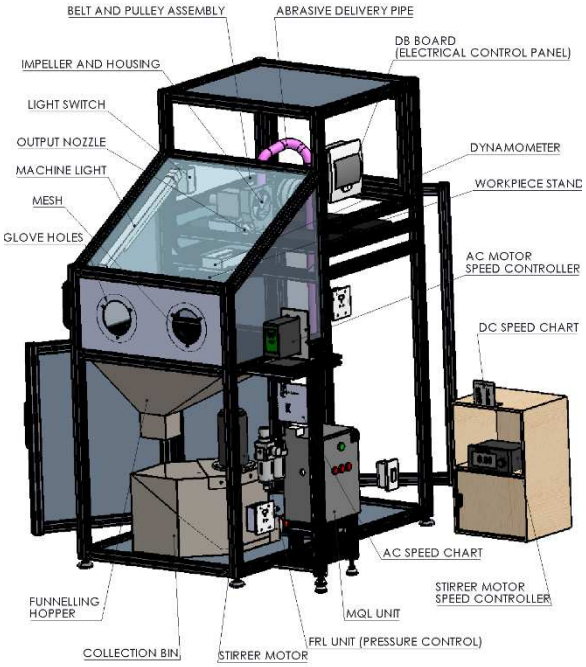

Fig 3 *- Labelled Blast Polishing Machine, Developed at the Advanced Manufacturing Lab – University of Cape Town*

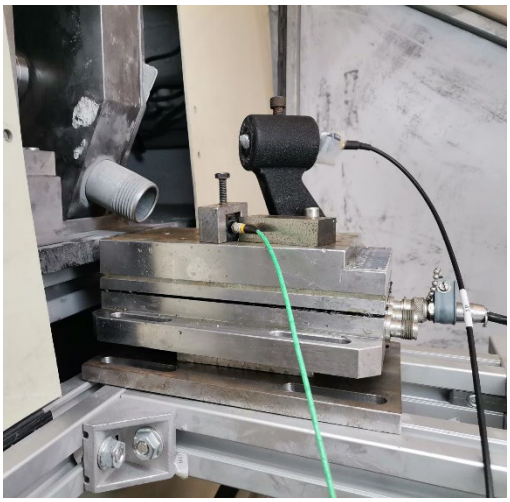

Fig 5 *- Experimental Set-Up*

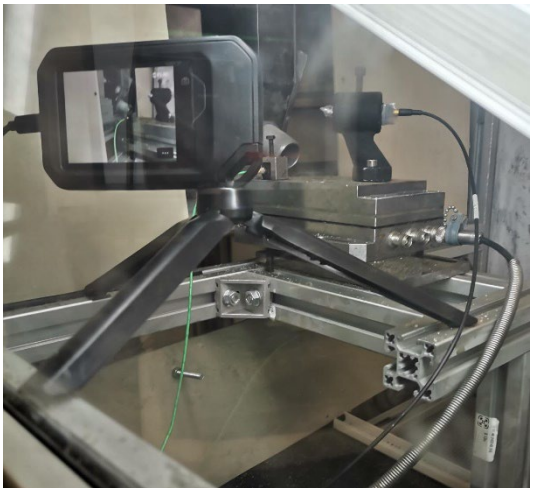

Fig 4 *- Experimental Set-Up with Video*

After initial polishing characterization and verification was complete, the collection of force data was required. An experimental set-up (see **Fig 5**) was created by using data-acquisition tools. A workpiece stage was developed to hold a Kistler dynamometer at the required standoff distance (20mm) from the output nozzle (where the media is shot out by the impeller). An accelerometer, AE sensor and video camera were set up as well in to acquire the most data possible. DeweSoft

Fig 6 *- Unpolished (Left) vs. Polished (Right) South African Five Rand Coin*

X3 was used to collect data for varying impinging velocities (6.28m/s, 15m/s and 31.4m/s) and hydration levels (0%, 10%, 30%, 50%).

It is also important to note the abrasive media properties used in the experiment [6]:

Table 1 *- Material Properties of Abrasive Constituents*

	Gelatin	SiC	Diamond	Water
Constituency (%)	47, 67, 87 or 97	2.9	0.1	0, 10, 30 or 50
Density	680	3020	3500	997
Diameter	1 mm	2.5 µm	2.5 µm	N/A
Elastic Modulus	43.2 kPa	330 GPa	1100 GPa	N/A
Poisson's Ratio	680	3020	3500	0.5

The figure below shows a microscopic image (32x magnification) of the gelatin core used and shows diameter measurements across the length of the abrasives.

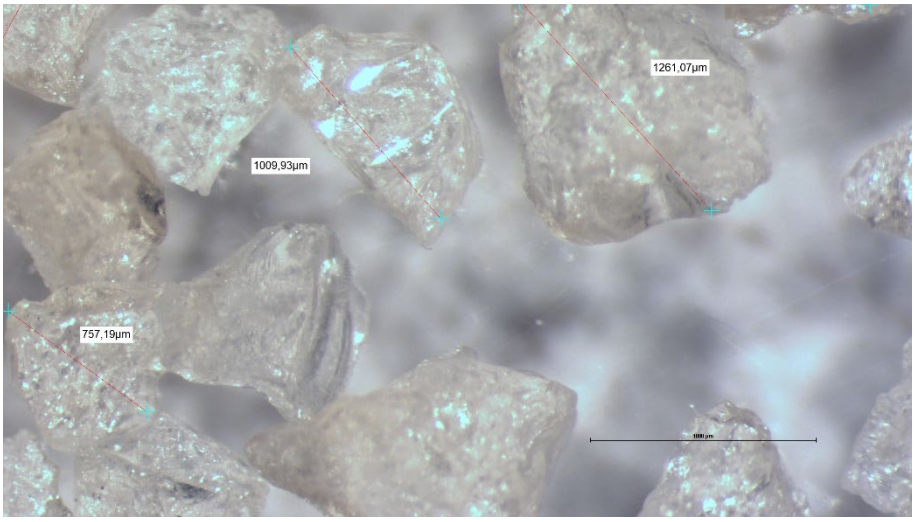

Fig 7 *- Gelatin Microscopic Image*

The following measurements were made for impact force (an average of 3 experiments for each condition):

Table 2 *- Experimentally Measured Forces*

	6.28m/s	15m/s	31.4m/s
10%	1.822 N	2.463 N	3.744 N
30%	1.597 N	1.990 N	3.318 N
50%	1.467 N	1.650 N	2.757 N

This is visually represented in **Fig 8** below.

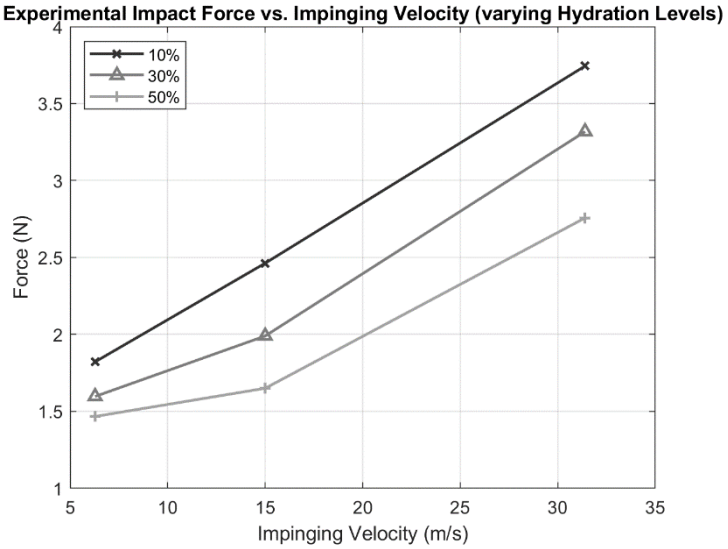

Fig 8 *- Experimentally Measured Impact Forces*

Using multivariate linear regression, we acquire the following empirical equation for force as a function of both hydration and impinging velocity:

$$F_{imp} = 1.6876 - 0.01796H_{\%} + 0.066759V_{imp} \quad (7)$$

Note that hydration should be substituted in as its representative number instead of a percentage of 100 i.e., 50 instead of 0.5.

3 Force Model and Material Properties

To make an adequate comparison, kinetic energy is matched over hydration levels and is increased based on the dry impinging velocities. Mass increases as hydration is increased and thus the velocity of impact is lessened as hydration is increased (thereby keeping a constant kinetic energy).

The dry abrasive mass is found by assuming a spherical abrasive, knowing the radius of the abrasive, and knowing the density of the abrasive. This gives a mass of:

0.35605mg (at a radius of 0.5mm)

At dry impact, the impinging velocities vary are taken at the following intervals: 6.28 m/s, 15m/s, 31.4m/s, 45 m/s and 60 m/s. This corresponds to kinetic energies of: 0.07 mJ, 0.040 mJ, 0.175 mJ, 0.3605 mJ and 0.6409 mJ.

Velocities (m/s) for increasing hydration levels are then found to be:

Table 3 *- Impinging Velocities at Various Hydration Levels for Constant Kinetic Energies across Hydration Levels*

10% Hydration				
5.9877	14.3019	29.9387	42.9058	57.2078
30% Hydration				
5.2516	12.5436	26.2580	37.6309	50.1745
50% Hydration				
4.8890	11.6775	24.4449	35.0325	46.7099

Abrasive properties used in this model are as stipulated in the previous section. Workpiece properties used are: 113 GPa for the elastic modulus of Ti6Al4V and 0.342 for the Poisson ratio of Ti6Al4V [6].

The last important derivation of material property to acquire is that of the variation in elastic modulus and density while increasing hydration. Elastic modulus is a measure of object stiffness. Fukumoto et al. [13] measured its change (the static modulus of abrasive) as wetness was increased. For a wetness of 0%, 10%, 30% and 50%, they found Elastic modulus to be: 43.2kPa, 7.8kPa, 0.78kPa and 0.52kPa respectively. Using the law of mixtures, the elastic modulus of the abrasive is determined by:

$$E_{abr} = \left(\frac{\%_{water}}{E_{water}} + \frac{\%_{gelatin}}{E_{gelatin}} + \frac{\%_{SiC}}{E_{SiC}} + \frac{\%_{diamond}}{E_{diamond}}\right)^{-1} \quad (8)$$

Using the determined elastic modulus from Fukumoto et al., we find that water has a contributing elastic modulus of approximately 0.9kPa and leads to the following output:

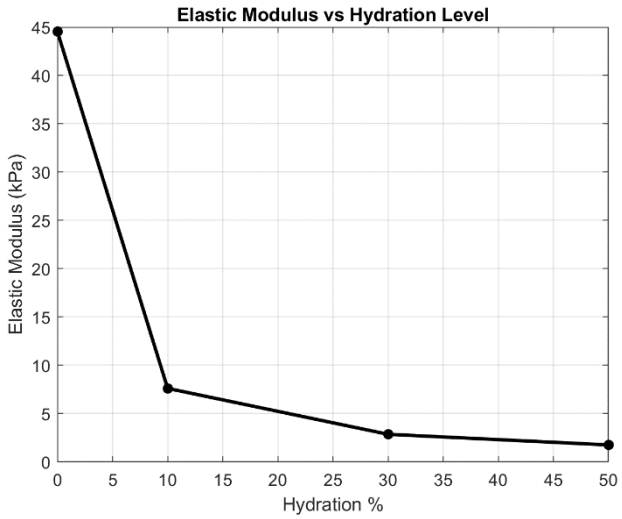

Fig 9 *- Elastic Modulus of Abrasive as a Variation of Hydration Level*

Note that density is found in using the same equation by replacing all values of elastic modulus with density.

After material property analysis, a model for force can be developed. Adaptations and modifications have been made to a previously developed model [6] (by the authors) to ascertain the contact forces for various hydration levels (at multiple kinetic energies). The model is based on sets of developed and verified empirical formulae as well as hertzian contact mechanics. Derivations based on the notion of critical values (the point at which a material changes behavior from elastic to plastic) were made, and the output of impinging force at a particular kinetic energy (and relative impinging velocity) was determined to be:

$$F_{imp} = F_c \left(\frac{\omega(V)}{\omega_c}\right)^{3/2} \tag{9}$$

While F_{imp} can also be calculated by the widely used (by substituting $w(V)$ into the equation) [18]:

$$F_{imp} = \frac{4}{3} E' \sqrt{R} [w(V)]^{3/2} \tag{10}$$

Where:

$$F_c = \frac{4}{3}\left(\frac{R}{E'}\right)^2 \left(\frac{C}{2}\pi S_y\right)^3 \tag{11}$$

$$\omega_C = \left(\frac{\pi C S_y}{2E'}\right)^2 R \tag{12}$$

$$\omega(V) = \left(\frac{5V^2 m_{abr} \omega_c^{3/2}}{4F_c}\right)^{2/5} \tag{13}$$

E' is the combined elastic modulus of the workpiece and abrasive:

$$\frac{2}{E'} = \frac{1-v_1^2}{E_1} + \frac{1-v_2^2}{E_2} \tag{14}$$

v_1 and v_2 are workpiece and abrasive poisson's ratios respectivelly and E_1 and E_2 are workpiece and abrasive elastic moduli respectivelly. R is the radius of the abrasive (combined abrasive is not applicable if the assumption of sphere interacting with a plane is true). C is the critical yield stress coefficient:

$$C = 1.295e^{0.736v} \tag{15}$$

S_y is the yield strength of the abrasive (210kPa [6]). V is the impinging velocity of the abrasive upon the workpiece. m_{abr} is the abrasive particle's mass. Note that critical velocity is given by:

$$V_c = \sqrt{\frac{4\omega_c F_c}{5m_{abr}}} \tag{16}$$

The ratio of impinging velocity to critical velocity is important as it ensures that the use of the developed model is applicable. If V/V_c is greater than 1, the equations cannot be used as the collision would incur plastic deformation. For all values of hydration and maximum impinging velocities, the ratio is less than 1 and therefore these equations are applicable.

Contact area can be estimated by:

$$A = A_C\omega(V) \tag{17}$$

Which allows for the estimation of contact stress by the typical contact stress equation for a plane interacting with a sphere:

$$\sigma = \frac{1.5F_c}{A} \tag{18}$$

Contact area is also assumed as circular and thus contact area equals:

$$A = \pi a^2 \tag{19}$$

Where a is the radius of circular contact, and from contact mechanics, the area of contact can be expressed in terms of deformation:

$$A = \pi(2\delta R - \delta^2) \tag{20}$$

Knowing the abrasive size and density, we can calculate the volume and associated mass for different water contents (as water content is a direct function of abrasive mass):

$$V_{abr} = \frac{4}{3}\pi R_{abr}^3 \tag{21}$$

$$m_{abr} = (1 + H\%)\rho_{abr}V_{abr} \tag{22}$$

It is important to note that with varying hydrations, the mass, radius, density and elastic modulus of the combined abrasive change as follows:

Table 4 *- Abrasive Properties at Various Hydration Levels*

$m_0 = 0.356\ mg$	$\rho_0 = 680\ kg/m^3$	$R_0 = 0.500$ mm	$E_0 = 43.2$ kPa
$m_{10} = 0.392\ mg$	$\rho_{10} = 702\ kg/m^3$	$R_{10} = 0.512$ mm	$E_{10} = 7.61$ kPa
$m_{30} = 0.509\ mg$	$\rho_{30} = 752\ kg/m^3$	$R_{30} = 0.545$ mm	$E_{30} = 2.87$ kPa
$m_{50} = 0.5875\ mg$	$\rho_{50} = 809\ kg/m^3$	$R_{50} = 0.558$ mm	$E_{50} = 1.765$ kPa

Change in radius can be calculated by assuming the abrasive is spherical in nature and then deriving the radius from the mass:

$$r = \sqrt[3]{\frac{3m}{4\rho\pi}} \tag{23}$$

Elastic modulus and density vary as mentioned previously.

It was found the force decreases logarithmically (with a sharp initial decrease) as hydration level is increased, while force increases logarithmically (with a gentle initial increase) as kinetic energy is increased. See below for a visual representation. The values and trends agree well with the measured experimental forces as well as by those stipulated by Fukumoto et al.

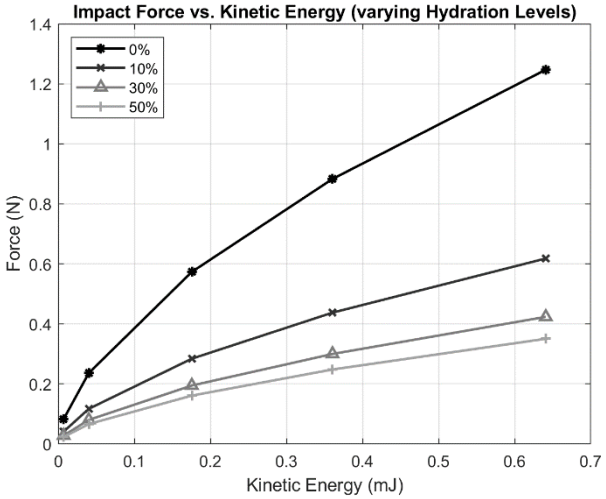

Fig 10 *- Impact Force as a Function of Kinetic Energy (for various hydration levels)*

Calculations for contact time could then be complete (in order to establish the damped frequency of contact for the vibrational model). These were acquired by dividing the product of the respective velocity (at a particular kinetic energy) and abrasive mass by the impinging force of the abrasive:

$$t_{contact} = \frac{m_1 v_1}{F_{imp}} \tag{24}$$

Contact time shows a logarithmic decay as kinetic energy is increased (tending towards a limit as energy increases). Contact time increases greatly as hydration is increased (with a large step occuring between 10% and 30%).

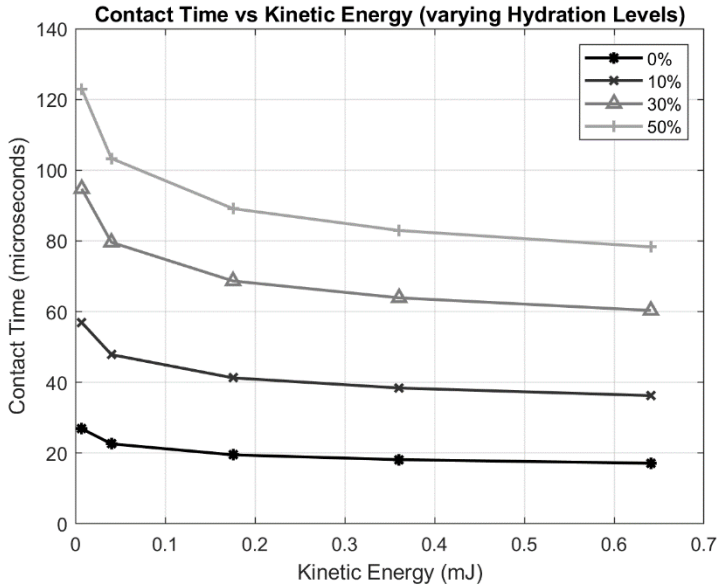

Fig 11 *- Contact Time as a function of Kinetic Energy (for varying hydration levels)*

4 Spring Dashpot Model

In addition to the multi-layered nature of the multi-con abrasive (gelatin-SiC-diamond), an incredible variety of effects can be achieved with minimal changes to the process design, by manipulating abrasive parameters. The below model is an attempt at characterizing the effect of hydrating the abrasive to different levels, firstly to prove that the addition of moisture aids in reducing contact stress and thus enables ductile regime polishing conditions to occur at higher than usual velocities, and secondly: to create a series of relations and inputs for further research to occur (namely that of defined damping ratios and damping coefficients).

4.1 Basis of Model and Assumptions

Fig 12 below shows the model used at further analysis, where m represents the mass of the abrasive, c represents the damping due to hydration (a desired output of this research), k represents the combined stiffness of the abrasive system, and x represents the deformation of the abrasive. The fixed ground is assumed as the workpiece of the material (which in this case would be a flat SLM produced Ti-6Al-4V component). As per the Kelvin-Voigt model, an undamped free vibration

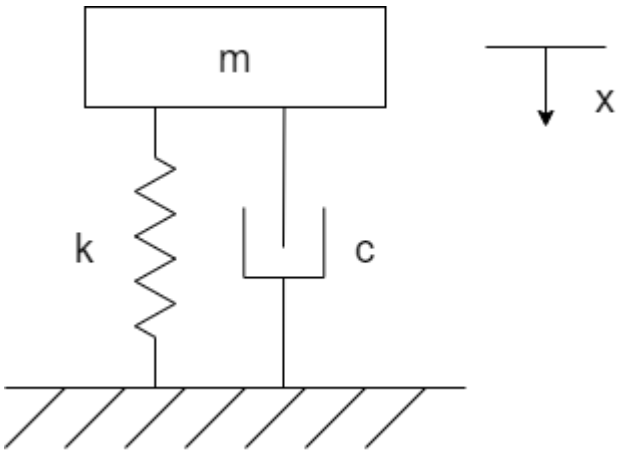

Fig 12 *- Spring-Dashpot Model for Wet Contact*

is chosen as the basis of this model as it incorporates the necessary system parameters (creep), while lessening complications in process design.

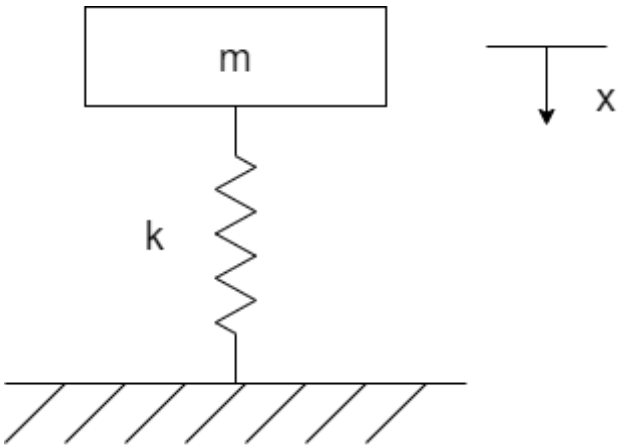

Fig 13 *- Spring Model for Dry Contact*

Fig 13 above shows the first vibrational model used in this research (where the abrasive is assumed to not be hydrated at all). This allows for a slightly simpler solution which can then be modified to include hydration factors.

Fig 14 *- Figures Key*

Using the basis of Hooke's law, the estimation/assumption that spring stiffness is equal to the elastic modulus of the abrasive is made:

$$k_{abr} = E_{abr} \tag{25}$$

We then investigate the force balance as follows:

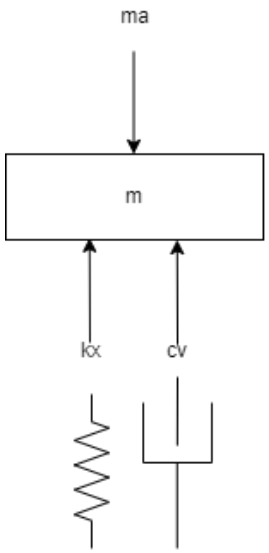

Fig 15 *- Force Balance on Spring Dashpot Model*

$$m\ddot{x} + c\dot{x} + kx = 0 \tag{26}$$

Simplified to:

$$\ddot{x} + 2\zeta\omega_n\dot{x} + \omega_n^2 x = 0 \tag{27}$$

Where:

$$\omega_n = \sqrt{\frac{k}{m}} = \sqrt{\frac{E}{m}} \tag{28}$$

Noting that the Elastic modulus and abrasive combined mass change as hydration changes, the natural frequency will change accordingly. Note that the damping ratio is given by the following equation:

$$\zeta = \frac{c}{2m\omega_n} \tag{29}$$

Where all variables are as stated previously (except t, which is time).

Damped frequency is described by:

$$\omega_d = \omega_n\sqrt{1-\zeta^2} \tag{30}$$

ω_d can be described as the period of contact (where displacement is 0 as contact begins, building up to the largest displacement *X* before the abrasive begins to return to its original shape and leave the workpiece). See **Fig 16** below:

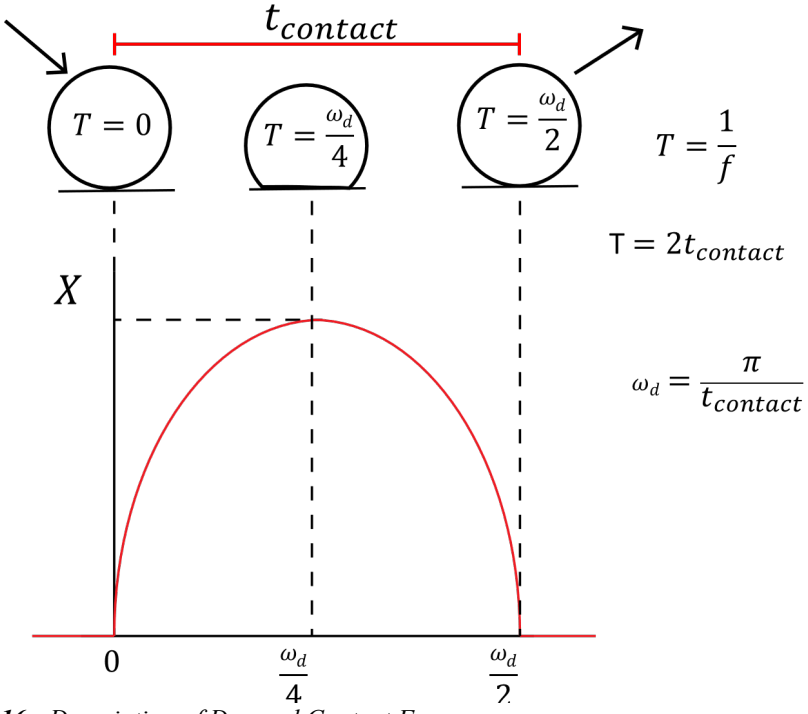

Fig 16 *- Description of Damped Contact Frequency*

The damped frequency can thus simply be described as:

$$\omega_d = \frac{\pi}{t_{contact}} \tag{31}$$

Where contact time is used as per Section 3.

Mass increases with hydration level as stated previously. This means that the natural frequency changes slightly (decreases) as hydration is increased. This implies that the damping coefficient (zeta) will change with varying hydrations. We know the contact times for each wetness and velocity increment. We can then determine contact period and frequency ratio for each hydration level.

Once the damped frequency and natural frequencies are solved for, the damping ratio (ζ) can be found by rearranging (30) to:

$$\zeta = \sqrt{1 - \left(\frac{\omega_d}{\omega_n}\right)^2} \tag{32}$$

While damping coefficient can be found by rearranging (29):

$$c = 2m\omega_n\zeta \tag{33}$$

After doing the force balance, displacement solutions can be acquired by using vibrational analysis, which leads to the following equation:

$$x(t) = A_1 \sin(\omega_d t)\, e^{-\zeta\omega_n t} + A_2 \cos(\omega_d t)\, e^{-\zeta\omega_n t} \tag{34}$$

Where: $x(t)$ is displacement ($\delta(t)$). $A_2 = 0$ because the initial displacement is x = 0. While:

$$A_1 = \frac{\dot{x}_o}{\omega_d} \tag{35}$$

x is a measure of the deformation δ and thus as previously stated we can find the contact stress by:

$$\sigma = \frac{1.5F_c}{\pi(2\delta R - \delta^2)} \tag{36}$$

4.2 Undamped (dry) contact Displacement

When damping is not present (as in Figure 2), the damping frequency is not present and the only present frequency is that of natural frequency, leaving the displacement solution as:

$$x = \frac{\dot{x}_o}{\omega_n} sin(\omega_n t) \tag{37}$$

The contact times for an undamped abrasive can be found at various kinetic energies by using the times stated in Section 3. We can then get the maximum displacement at various kinetic energies ($sin90° = 1$, therefore we can omit the sin term for maximum displacement). This easily lets us acquire contact stress from (36).

4.2 Damped (wet) Contact Displacement

Now that we have the undamped case completed, we need to calculate the displacements (and subsequently the contact areas and contact stresses) for varying hydration levels. This is slightly more complex in nature than the undamped solution.

We can continue our vibrational analysis by first finding coefficient A_1 for each hydration level and associated kinetic energy. We can then find the maximum displacements for each case. Displacements are found by (34).

Finally, we can calculate the contact stresses for each level of hydration along with its associated kinetic energy.

5 Vibrational Model Results and Discussion

The three main results of this analysis (damping ratio, damping coefficient and contact stress) are shown and discussed in this section, with a focus on how the outputs affect the blast polishing process and what they mean to future designs.

The first output of this model is that of damping ratio. **Fig 17** below shows that the damping ratio at low kinetic energies is close to critical ($\zeta = 1$) and shows the trend of logarithmic decrease as kinetic energy is increased (becoming more underdamped). Lower damping ratios imply longer stabilization times as well as more oscillations before equilibrium is reached (therfore higher displacements). This analogy aligns well with the results from previous research, as higher hydrations mostly result in greater displacements and greater contact times. This also aligns with the previous section which shows that higher contact times are associated with higher hydration levels and lower kinetic energies.

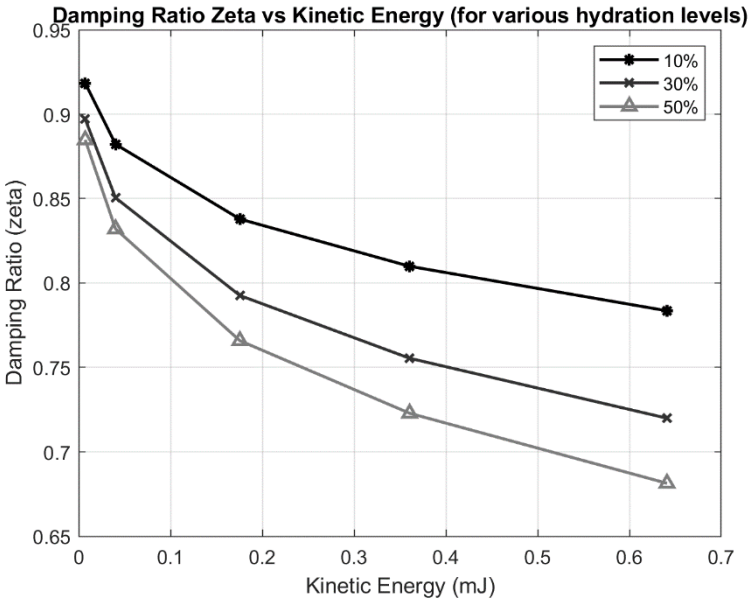

***Fig 17** - Damping Ratio Results*

Damping coefficient is relative to the system as mass plays a large role in its determination and it can vary from case to case, but the results (**Fig 18**) show that damping coefficient has a similar trend to damping ratio (with more dramatic decreases as hydration is increased), which helps to affirm the previously discussed results.

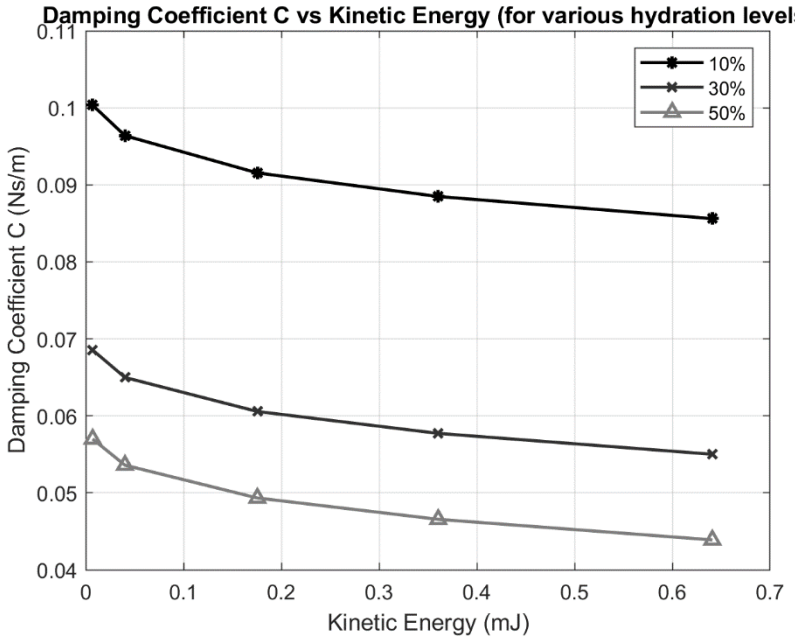

Fig 18 *- Damping Coefficient Results*

An important result of the vibrational analysis (which serves as an input for a large array of contact mechanic relations) is that of contact deformation. This was calculated in the previous section and plotted over time, however, in contact mechanics, the deformation of interest is that of maximum deformation (which is when the abrasive will be applying maximum force upon the workpiece). **Fig 19** below shows that deformation increases logarithmically (with a sharp initial gradient) as kinetic energy is increased. Dry contact deformation does not bare much difference to 10% hydration contact deformation; however, 30% and 50% hydration show great increases in deformation (approximately 1.7x and 2.3x increases respectively). This is due to the great reduction in stiffness as well as the lower damping ratios. Again, the results match those of Fukumoto et al. [13].

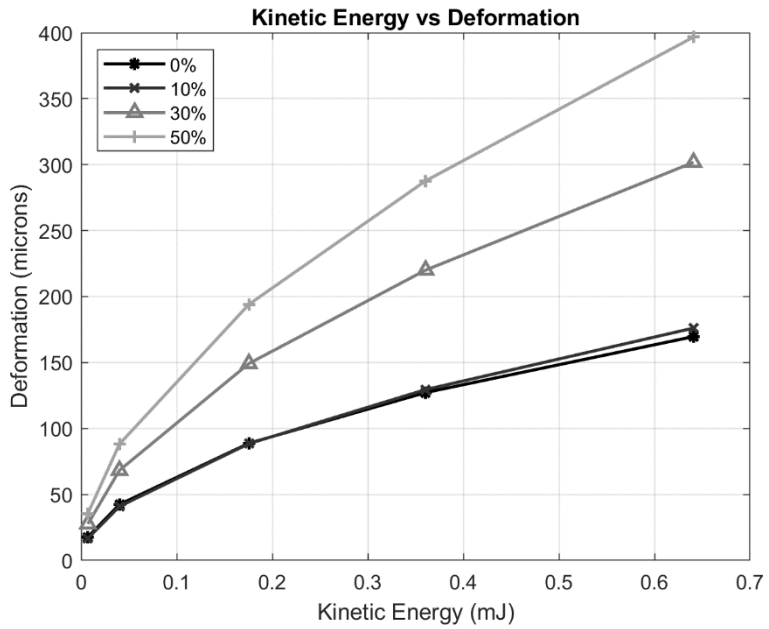

***Fig 19** - Deformation as a function of Kinetic Energy (for various hydration levels)*

Finally, and of interest to the material removal mechanism, the results of contact stress are shown (**Fig 20**). The results are displayed as a unitless function of dry contact stress to adequately show the effect of hydration and kinetic energy on contact stress. Unitless presentation is also selected because the micro and nano contact stresses (between diamond/SiC and Ti6Al4V asperities), which cause the most abrasive removal by ductile polishing, cannot be separated in this model (which accounts for the viscoelastic contact of gelatin, while SiC and diamond barely contribute to the overall system stiffness). In agreement to the displacement results, the contact stress drops minorly when using 10% wet abrasives and then becomes much smaller at 30% and 50% (approximately 25% and 18% of the dry contact, respectively). Kinetic energy plays much less of a role in the determination of contact stresses at higher hydrations and this shows that greater damping is occurring at higher levels of hydration.

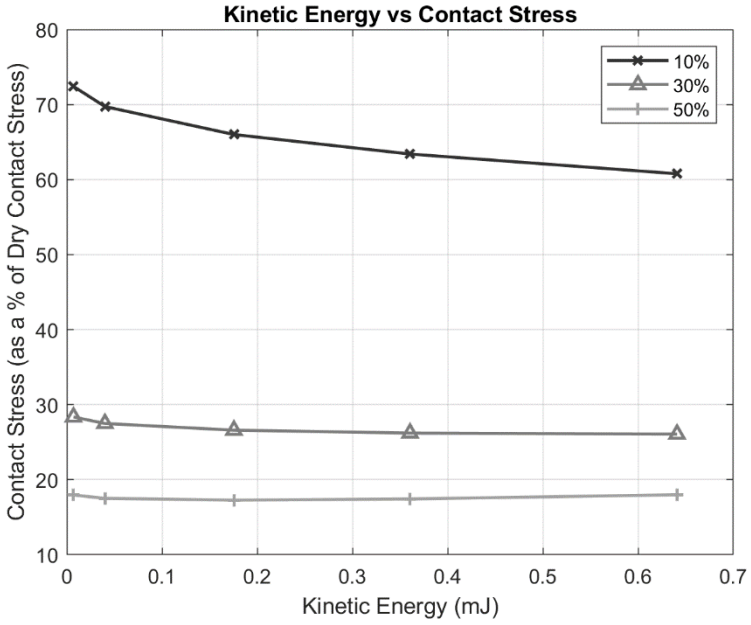

Fig 20 *- Contact Stress (as a percentage of dry contact stress) as a function of Kinetic Energy (for various hydration levels)*

6 Conclusion

This paper has presented a linear viscoelastic model for the blast polishing of Ti6Al4V surfaces, with experimental results presented along with an adapted empirical-analytical force model (based on Hertzian contact mechanics and the notion of critical value) to account for varying kinetic energies of impact and hydration levels of abrasive. The results of the force model agree with experimental research presented as well as with experiments done by other authors on blast polishing [13]. Impact forces were found to decrease dramatically with increases in hydration levels (1.3N at 0% hydration to 0.35N at 50% hydration, for the highest levels of kinetic energies), while increasing logarithmically with kinetic energy. Contact times were inferred using conservation of momentum and were found to increase significantly as hydration levels are increased (from 18μs to 78μs for highest kinetic energies at 0% and 50% hydrations, respectively).

Damping ratios were found to be close to critical at low values of kinetic energy while they rapidly became more underdamped as kinetic energy was increased. Higher values of hydration also result in lower values of damping ratio and the same trend was detected in the damping coefficient.

Maximum contact deformation was found to be similar for dry contact and 10% wetness, before dramatically increasing when wetness was increased to 30% and 50%. This analogy again agrees with that of experimental studies and the force model. Contact stress decreases significantly as hydration levels are increased (25% of dry contact at 30% and 18% of dry contact at 50%). This proves that higher hydration aids in allowing a polishing process to occur at higher velocities, while imparting less damage to the surface of the workpiece.

The work completed here hopes to aid in the development of further models in the blast polishing process and to making the process more attractive to the manufacturing industry.

Declarations

- **Ethical Approval:** The author(s) confirm that the paper has not been published previously in any form or language, that it is not under consideration for publication elsewhere and does not contain material which has been published previously. The results are presented clearly, honestly, and without fabrication, falsification, or inappropriate data manipulation.
- **Consent to Participate:** Not applicable
- **Consent to Publish:** Not applicable
- **Authors Contributions:** Quintin de Jongh: Writing Original Draft, Investigation, Conceptualization, Methodology, Machine/Process Design and Development, Experimentation, Model Development, Validation. Ramesh Kuppuswamy: Supervision, Project administration, Resources, Validation and Investigation, support writing. Matthew Titus: Conceptualization, Machine/Process Design and Development, Investigation.
- **Funding:** This project was supported by fund NRF GRANT: INCENTIVE FUNDING FOR RATED RESEARCHERS (IPRR) –South Africa through Reference: RA191118492767 and Grant No: 136118. The views expressed and the conclusions drawn in this paper are those of the authors and cannot necessarily be attributed to the references.
- **Competing Interests:** The author(s) declared no potential conflicts of interest with respect to the research, authorship, and/or publication of this article.
- **Availability of data and materials:** The authors confirm that the data supporting the findings of this study are available within the article.

References

[1] Kuppuswamy R, Ozbayraktar S, Saridikmen H (2012) Aero-lap polishing of poly crystalline diamond inserts using Multicon media. *Journal of*

Manufacturing Processes 14(2):167-173. https://doi.org/10.1016/j.jma-pro.2011.12.003

[2] Nizar M (2016) Influence of surface modification by blast polishing method on the cutting performance of carbide tool. Toyohashi University of Technology, Doctoral Dissertation.

[3] Nishimuraa Y, Endob M, Yanaseb K, Ikedab Y, Miyakawaa S, Miyamotoa N (2016) High cycle fatigue strength of spring steel with small scratches. *Proceedings of First Structural Integrity Conference and Exhibition*, Bangalore

[4] Huang H, Gong Z, Chen X, Zhou L (2002) Robotic grinding and polishing for turbine-vane overhaul. *Journal of Materials Processing Technology* 127(2):140-145. https://doi.org/10.1016/S0924-0136(02)00114-0

[5] Kitajima K, Yamamoto A (2010) Latest Trends in Deburring Technology. *International Journal of Automation Technology* 4(1):4-8. doi:10.20965/ijat.2010.p0004

[6] de Jongh Q, Kuppuswamy R, Titus M (2022) A Force Controlled Polishing Process Design, Analysis and Simulation Targeted at Selective Laser Melted Ti6Al4V Aero-Engine Components. *International Conference on Competitive Manufacturing*, Stellenbosch.

[7] Wang M, Qin P, Zan T, Gao X, Han B, Zhang Y (2021) Improving optimal chatter control of slender cutting tool through more accuraate tund mass damper modeling. *Journal of Sound and Vibration* 513:1-16. https://doi.org/10.1016/j.jsv.2021.116393

[8] Naghieh G, Rahnejat H, Jin Z (1997) Contact mechanics of viscoelastic layered surface. *Transactions on Engineering Sciences* 14:59-68. doi: 10.2495/CON970071

[9] Assie A, Eltaher M, Mahmoud F (2010) Modeling of viscoelastic contact-impact problems. *Applied Mathematical Modelling* 34:2336-2352. https://doi.org/10.1016/j.apm.2009.11.001

[10] Hunek I (1993) On a penalty formulation for contact-impact problems. *Comput. Struct.* 48(2):193-203. https://doi.org/10.1016/0045-7949%2893%2990412-7

[11] Fahmy M (2000) A Computational Model for Elastic-plastic Dynamic Contact, Ph.D Dissertation. Zagazig University, Doctoral Dissertation.

[12] Lopez-Guerra E.A, Solares S.D (2014) Modelling viscoelasticity through spring-dasphot models in intermittent-contact atomic force microscopy. *Beilstein Journal of Nanotechnology* 5:2149-2163. https://doi.org/10.3762/bjnano.5.224

[13] Fukumoto M, Takai K, Nizar M, Arimatsu N, Uemura M (2016) Study on polishing mechanism of cemented carbide by blast polishing. 3rd Report: Influence of water content in polishing media on polishing mechanism. *Journal of the Abrasive Processing Society* 60(5):261-266. https://doi.org/10.11420/jsat.60.261

[14] Bulicek M, Malek J (2012) On Kelvin-Voigt Model and its Generalizations. *Evolution Equations and Control Theory* 1(1):17-42. http://dx.doi.org/10.3934/eect.2012.1.17

[15] Roberts J, Jones R, Rothberg S (2001) Measurement of contact time in short duration sports ball impacts: an experimental method and correlation with

the perceptions of elite golfers. *Sports Engineering* 4: 191-203. http://dx.doi.org/10.1046/j.1460-2687.2001.00084.x

[16] Hocknell A (1998) Computational and Experimental Anlysis of Elastic Deformation in Impact, PhD Thesis. Loughborough University, Doctoral Dissertation.

[17] Goldsmith W (1960), Impact: the Theory and Physical Behaviour of Colliding Solids, Edward Arnold (Publishers) Ltd., London.

[18] Jackson R, Ghaednia H, Lee H, Rostami A (2013) Contact Mechanics, Tribology for Scientists and Engineers, Springer Science+Business Media, New York.

Supplementary Files

This is a list of supplementary files associated with this preprint. Click to download.

- DAQForces.xlsx